Journal of Colloid and Interface Science 657 (2024) 788–798

Contents lists available at ScienceDirect

Journal of Colloid And Interface Science

journal homepage: www.elsevier.com/locate/jcis

Highly biocidal poly(vinyl alcohol)-hydantoin/starch hybrid gels: A "Trojan Horse" for *Bacillus subtilis*

Vanessa Rosciardi [a,b], Damiano Bandelli [a], Gavino Bassu [a,b], Ilaria Casu [a], Piero Baglioni [a,b,*]

[a] Department of Chemistry "Ugo Schiff", University of Florence, Via della Lastruccia 3, 50019 Sesto Fiorentino (Florence), Italy
[b] CSGI, Center for Colloids and Surface Science, University of Florence, Via della Lastruccia 3, 50019 Sesto Fiorentino (Florence), Italy

GRAPHICAL ABSTRACT

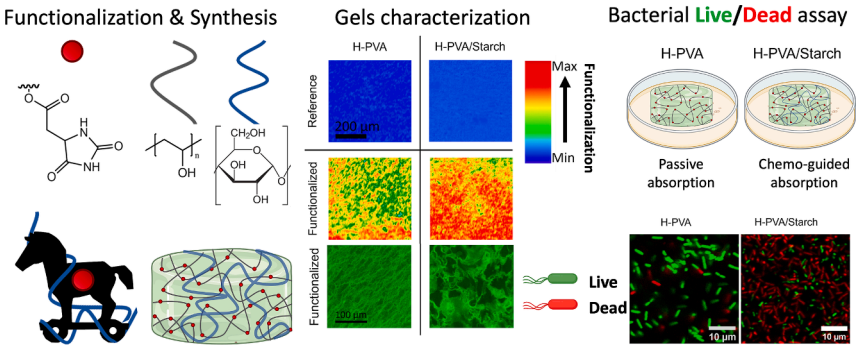

ARTICLE INFO

Keywords:
PVA
Starch
Cryogel
Trojan Horse
Hydantoin
Anti-bacterial

ABSTRACT

Hypothesis: Poly (vinyl alcohol) (PVA) cryogels can be functionalized with *n*-Halamines to confer biocidal features useful for their application as wound-dressing tools. Their efficacy can be boosted by stably embedding a polymeric bacterial food source (e.g., starch) in the gel matrix. The bioavailability of the food source lures bacteria inside the gel network via chemotactic mechanisms, promoting their contact with the biocidal functionalities and their consequent inactivation.

Experiments: The synthesis of a novel hydantoin-functionalized PVA (H-PVA-hyd) is proposed. The newly synthesized H-PVA-hyd polymer was introduced in the formulation of H-PVA-based cryogels. To promote the cryogelation of the systems we exploited phase-separation mechanisms employing either a PVA carrying residual acetate groups (L-PVA) or starch as phase-segregating components. The permanence of the biocidal functionality after swelling was investigated via proton nuclear magnetic resonance (^{1}H NMR) and Fourier transform infrared (FT-IR) microscopy. The activated H-PVA-hyd cryogels have been tested against bacteria with amylolytic activity (*Bacillus subtilis*) and the outcomes were analyzed by direct observation via confocal laser scanning microscopy (CLSM).

Findings: The cryogels containing starch resulted in being the most effective (up to 90% bacterial killing), despite carrying a lower amount of hydantoin groups than their starch-free counterparts, suggesting that their improved efficacy relies on a "Trojan Horse" type of mechanism.

* Corresponding author at: Department of Chemistry "Ugo Schiff", University of Florence, Via della Lastruccia 3, 50019 Sesto Fiorentino (Florence), Italy.
E-mail addresses: vanessa.rosciardi@unifi.it (V. Rosciardi), damiano.bandelli@unifi.it (D. Bandelli), gavino.bassu@unifi.it (G. Bassu), ilaria.casu@stud.unifi.it (I. Casu), baglioni@csgi.unifi.it (P. Baglioni).

https://doi.org/10.1016/j.jcis.2023.11.142
Received 21 August 2023; Received in revised form 22 November 2023; Accepted 22 November 2023
Available online 27 November 2023

1. Introduction

Poly(vinyl alcohol) (PVA) is a water-soluble biodegradable "green" polymer characterized by extremely low cytotoxicity and excellent biocompatibility [1]. For its features, PVA has been widely used in the formulation of hydrogels for a variety of biomedical applications ranging from the realization of artificial organs to the synthesis of drug delivery devices and wound dressing materials [2]. For the latter purpose, PVA gels prepared via the freeze-thawing method (i.e., PVA cryogels, PVA-Cs) have gained particular attention thanks to their mechanical and physicochemical properties. [3] Moreover, their synthesis is free from chemical intermediates and hence ensures the non-toxicity of the application. Indeed, PVA-Cs are obtained by subjecting PVA aqueous solutions to cycles of freezing and thawing, during which hydrogen bonds are formed between the —OH residues on the PVA chains, leading to the formation of crystalline domains that act as crosslinking points in the network. The resulting system is a strong "chemical-like" gel, obtained with no use of crosslinking agents or organic solvents. [4] Given to their flexibility, tissue-like water content, and mild adherence, PVA-Cs are highly tolerated on wounded skin and are also particularly indicated in the treatment of chronic wounds, thanks to their ability to maintain an appropriate moisture balance in the wound bed, hence promoting autolytic debridement while giving cooling and analgesic effects. [5] To further promote the healing process, cryogels for wound dressing should be able to ensure a sterile environment since, together with other processes (*e.g.*, prolonged expression of proinflammatory cytokines, modified expression of proteases, and high levels of oxidative stress[6]). Bacteria proliferation with consequent biofilm formation can strongly interfere with the correct healing of regular wounds, eventually favoring their evolution into chronic wounds. [7] Protection from bacteria proliferation can be ensured by loading the cryogel with antibiotics [8,9] or broad-spectrum disinfectants (e.g., hydrogen peroxide, [10,11] sodium hypochlorite, [12] and chloroxylenol-based solutions[13]). However, in the former case, some issues may arise in the treatment of bacteria that are prone to developing antibiotic resistance, [14,15] while in the latter the nonspecific action of the disinfectant (most of them expressing their biocidal effect via generic oxidative mechanisms) can cause damage to the patient's cells. [16,17].

An alternative approach to confer biocidal activity to PVA-based cryogels is to covalently bind molecules with antimicrobial activity directly to the PVA polymeric backbone. Given their high efficacy, low toxicity, and selectivity towards bacteria, molecules belonging to the group of *N*-halamines are particularly appropriate for the scope. [18,19].

N-halamines are a class of molecules characterized by the presence of one or more nitrogen-halogen covalent bonds in their structure, usually formed upon the halogenation of N—H precursors (i.e., imide, amide, or amine groups) [20]. The biocidal properties of *N*-halamines are due to the peculiar nature of the *N*—X bond (with X being the halogen, most commonly Cl and I), where the halogen atom formally displays the oxidation state + 1. The *N*—X bonds can hydrolyze in the presence of water and be reduced to N—H bonds, while the oxidative halogens react directly with the bacterial cells, compromising their vitality [21]. Hence, *N*-halamines do not induce antibiotic resistance [22] and, contrary to broad-spectrum disinfectants, their oxidation mechanism is activated only by the presence of bacteria, granting *N*-halamines good efficacy together with high selectivity towards the biological target. [23] *N*-halamines have been widely studied and applied as antimicrobial agents, and extensive reviews on the topic are available for interested readers. [19,23] Despite their popularity, little literature is available about *N*-halamines covalently linked to polymeric hydrogels, [18,24] and, as far as we know, no direct functionalization of PVA with *N*-halamines has been previously reported.

This contribution reports on the synthesis of a novel polymer with antimicrobial properties, obtained by covalently binding 5-hydantoin acetic acid (a cyclic *N*-halamine displaying two N—H sites) to a highly hydrolyzed PVA (H-PVA). The functionalized highly hydrolyzed PVA covalently bounded to hydantoin (H-PVA-hyd) was used to obtain PVA cryogels (twin chain hydrogels[25]) formed through a liquid–liquid phase separation in the presence of two PVA, differing for the molecular weight and hydrolysis degree (high molecular weight PVA, H-PVA, and low molecular weight PVA, L-PVA) or in the presence of starch, H-PVA/starch. The liquid–liquid phase separation process strengthens the continuous network of H-PVA and allows the fine tailoring of the morphological, mechanical, and viscoelastic features of the cryogels [25,26] (these concepts are illustrated with more detail in SI, Figure S1). The introduction of starch in the formed cryogel is particularly interesting since starch is a source of food for many bacterial strains. It is known that bacteria are capable of modifying their apparently random motion in response to changing environmental conditions [27]. As a result, bacteria can migrate toward the source of nutrients [28]. We show that starch has a direct impact on *Bacillus subtilis* mobility inside the gel networks that in our case translates into the possibility of actively attracting bacteria inside the matrix of the gel through a "Trojan Horse" mechanism, promoting their interaction with the biocidal molecules available in the gel's volume and the bacterial death.

2. Experimental

2.1. Materials

Poly (vinyl alcohol) with high hydrolysis degree (H-PVA, 99 % hydrolyzed, M_w 146–186 kDa), poly (vinyl alcohol) with lower hydrolysis degree (L-PVA, 88 % hydrolyzed, M_w 85–124 kDa), commercial rice starch (formally, a natural mixture of two different polymers, amylose, and amylopectin) were obtained from Sigma-Aldrich (Germany), Kurarai Co. Ltd. (Japan), and Kremer Pigmente (Germany), respectively. Anhydrous dimethyl sulfoxide (DMSO, anhydrous > 99.9 %), deuterated dimethyl sulfoxide (DMSO-d_6, purity > 99 %), 1-1′ carbonyl diimidazole (CDI, purity > 97 %), hydantoin-5-acetic acid (purity > 98 %), rhodamine 110 chloride (dye content ≥ 75 %), and sodium hypochlorite (NaClO, 10 % aqueous solution) were purchased from Sigma-Aldrich (Germany). Ethanol (EtOH, purity > 96 %) and acetone (purity > 97 %) were purchased from Carlo Erba (Italy). The *Bacillus subtilis* DMS-10 type strain (*B.subtilis*), used for the biocidal assessments was purchased in pellets from the Leibniz Institute DMSZ (Germany). All the reactants and materials were used as received and without further purification.

2.2. H-PVA functionalization reaction and product characterization

The two-step H-PVA functionalization reaction was conducted in anhydrous conditions. In the first step, equimolar amount of 1-1′ carbonyl diimidazole, CDI, and hydantoin-5-acetic acid were transferred in a round-bottom schlenk flask. Subsequently, DMSO was added to start the activation of carboxylic acid. The reaction between CDI and hydantoin 5 acetic acid led to the formation of the acyl-imidazole intermediate (scheme 1, panel A) with the formation of imidazole and CO_2 as side products. H-PVA was dissolved in a second round-bottom flask in DMSO at 70 °C. After complete dissolution, the acyl-imidazole was added to the PVA solution, and the esterification reaction was allowed to proceed for 6 h at 70 °C under moderate stirring.

The product was precipitated in 1:3 v/v "reaction mixture":ethanol at 4 °C. The solid product was dried, redissolved in water, precipitated from a 1:1 v/v ethanol:acetone mixture and dried in mild vacuum conditions. Samples of the purified product, as well as the starting reactants, were employed for both proton nuclear magnetic resonance (^{1}H NMR) and size exclusion chromatography (*SEC*) analyses. ^{1}H NMR experiments were performed in deuterated DMSO-d_6 at ambient temperature using a Bruker AVIII400 UltraShield Plus. For each experiment, 16 scans and 2 dummies were collected and the residual ^{1}H peak of the deuterated solvent was used for chemical shift referencing. *SEC* analyses

were performed utilizing a system composed of a Shodex ERC–3215α degasser connected with a Waters 1525 binary HPLC pump, a Waters 1500 series heater set at 40 °C, a Wyatt mini-DAWN TREOS detector (for multi-angle light scattering -MALS -detection), a Wyatt Viscostar–II detector (for viscosity measurements) and a Wyatt OPTILAB T–rEX detector (for refractive index-RI-measurements), a Shodex pre–column GPC K_D–G 4A and a Shodex column GPC K_D–806 M employing a 0.1 M NaCl solution in water as eluent with a flow rate of 0.6 mL min^{-1}. A set of polyethylene oxide standards (PEO, 3 kg $mol^{-1} < M_p < 969$ kg mol^{-1}) samples were purchased from PSS (PEOkit) and used for calibration. All data evaluation was performed according to standard procedures employing ASTRA software.

2.3. Gels' preparation and storage

Two sets of hydrogels were prepared via freeze-thawing. The first set contained non-functionalized H-PVA alone or with a second component (L-PVA or commercial rice starch, used without further purification). In the second set of samples, functionalized H-PVA-hyd was also introduced. The composition of the gel samples is summarized in Table 1.

The samples have been prepared as follows: the polymeric components were added in the specified proportions to ultrapure water in round-bottomed flasks and the suspensions were then kept at 98 °C to obtain a viscous solution. The solutions were poured into molds to obtain "flat" hydrogels (14 x 7 x 0.2 cm^3) and let cool to ambient temperature, kept at −20 °C overnight, and thawed. The obtained hydrogels were stored in ultrapure water for 1 week, to allow the release of the polymeric fraction not involved in the gel formation. All the hydrogels were stored at room temperature, and the storage water was changed daily.

2.4. Morphological characterization

Morphological characterization of the hydrogels was carried out employing confocal laser scanning microscopy (CLSM). Confocal images were acquired on gel samples swollen in solutions containing Rhodamine 110 chloride as the fluorescent probe. The images acquisition was carried out with a Leica TCS SP8 confocal microscope (Leica Microsystems GmbH, Wetzlar, Germany) using an Argon ion laser as the excitation source (λ = 488 nm) and a PMT detector (Photomultiplier Tube, selected detection range = 498–540 nm). A water immersion 63X/1.2 W objective (Zeiss) was used. All samples were placed in the sample-holder (Lab-Tek® Chambered Borosilicate Coverglass System, Nalge Nunc International, Rochester, NY, USA) before analysis. Bidimensional images obtained via CLSM of the hydantoin-functionalized hydrogels were furthermore analyzed to obtain the average dimensions of the gels' pores. The image analysis was performed using MorphoLibJ, a collection of mathematical morphology methods for ImageJ [29]. The 2D scans acquired by CLSM were converted into binary 8-bit images and then optimized to apply the "distance transform watershed" to distinguish individual pores [30].

Table 1
Gel samples compositions.

Sample	H-PVA (W/W)	L-PVA (W/W)	Starch (W/W)	H-PVA-Hyd (W/W)	Freeze-Thawing cycles
$H\text{-}PVA_{GEL}$	9 %	–	–	–	1
$H\text{-}PVA/L\text{-}PVA_{GEL}$	9 %	3 %	–	–	1
$H\text{-}PVA/Starch_{GEL}$	6 %	–	3 %	–	1
$H\text{-}PVA\text{-}hyd_{GEL}$	4.5 %	–	–	4.5 %	2
$H\text{-}PVA\text{-}hyd/L\text{-}PVA_{GEL}$	4.5 %	3 %	–	4.5 %	2
$H\text{-}PVA\text{-}hyd/Starch_{GEL}$	3 %	–	3 %	3 %	2

2.5. Residual hydantoin functionality after washing

After equilibration in water for 1 week, samples of the blank and functionalized gels were analyzed by means of Fourier-transform infrared (FT-IR) and ^1H NMR spectroscopy to assess the permanence of the hydantoin functionality in the gel networks. FT-IR spectra of gels were collected in attenuated total reflection (ATR) mode using a Thermo Nicolet Nexus 870 with an MCT detector (Mercury-Cadmium-Telluride). The spectra were recorded between 650 cm^{-1} and 4000 cm^{-1}, with a spectral resolution of 2 cm^{-1} and 128 scans for each spectrum. The permanence of hydantoin in the gel was qualitatively assessed by the presence of signals around 1720 cm^{-1} relative to the hydantoin C═O stretching modes of ester, amide, and imide groups [31], not present in H-PVA, L-PVA, and starch. Quantitative analyses were performed via ^1H

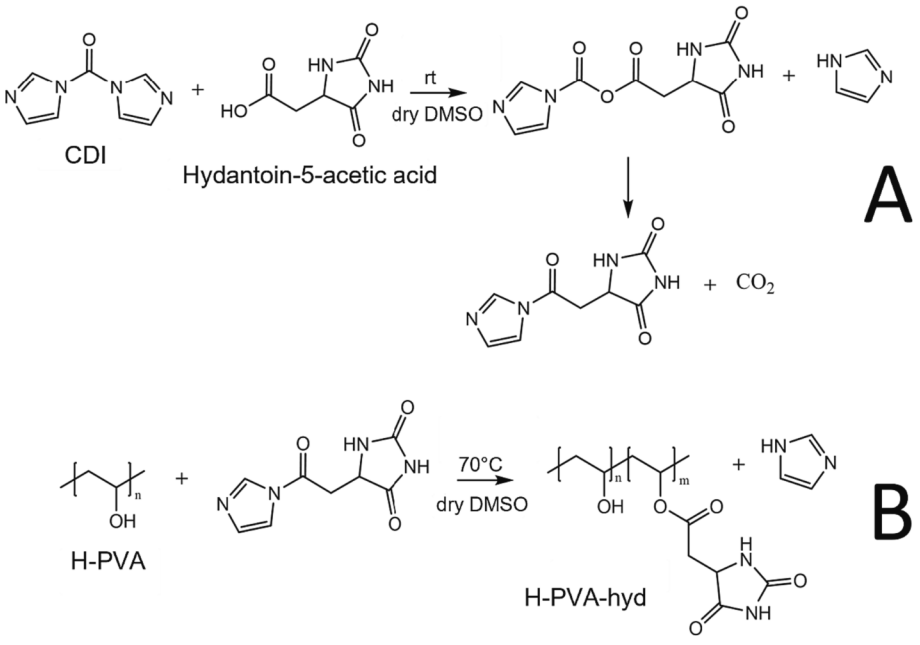

Scheme 1. Synthetic route toward the CDI-promoted functionalization of H-PVA with hydantoin-5-acetic acid.

NMR with the same experimental set-up described in section 2.2 (H-PVA functionalization reaction and product characterization).

2.6. Distribution of the hydantoin group in the gels

The hydantoin group distribution in the washed gels was determined by Fourier transform infrared microscopy (μFT-IR) mapping. The 2D μFT-IR imaging of freeze-dried samples was carried out using a Cary 620–670 FT-IR microscope, equipped with a Focal Plane Array (FPA) 128 x 128 detector (Agilent Technologies). This setup allows for the detection of analytes inhomogeneously distributed on surfaces at low local concentrations [25]. The spectra were collected in reflectance mode directly on the samples, with a spectral resolution of 8 cm^{-1} and 128 scans for each spectrum. The result of each acquisition consisted of a "single tile" map with dimensions of 700 x 700 μm^2, corresponding to 128 x 128 pixels. Each pixel has dimensions of 5.5 x 5.5 μm^2 and provides an independent spectrum. In each 2D map, the intensity of characteristic bands of C═O stretching at 1720 cm^{-1} was imaged. The chromatic scale of the maps shows increasing absorbance of the bands as follows: blue < green < yellow < red.

2.7. Rheological characterization

Rheological analyses were performed on flat gel samples (thickness ≈ 2 mm) after complete swelling. The viscoelastic properties of the hydrogels were studied using a Discovery HR-3 rheometer (TA Instruments) with a parallel plate geometry of 40 mm diameter and a Peltier temperature control system, Temperature was 25 °C for all the experiments). Amplitude sweep tests were carried out in a range of oscillation strains from 0.01 % to 100 % at a constant oscillation frequency (1 Hz). Frequency sweep tests (frequency range 1–100 Hz) were performed within the Linear Viscoelastic Region (LVE), which was previously determined through amplitude sweep tests. The results are presented as averages of three repeats.

2.8. Activation of the biocidal properties

Hydantoin functionalities display biocidal properties after their N—H groups are converted into *N*—X groups (with X = Cl, Br, I). In this study the H-PVA-hyd polymer was chlorinated after the formation of hydrogels by immersion of the H-PVA-hyd-containing gels in NaClO aqueous solutions. Two different protocols were used. The first one consisted of a 15-minute immersion of the gel sample in a 1 % NaClO solution. In the second protocol, the gels were immersed for a shorter time (30 s) at higher NaClO concentrations (10 %). In both procedures, after treatment, the gels were stored in ultrapure water for 48 h and the storage water was changed twice to remove unbound chlorine ions. The samples were then freeze-dried and analyzed by means of FT-IR ATR

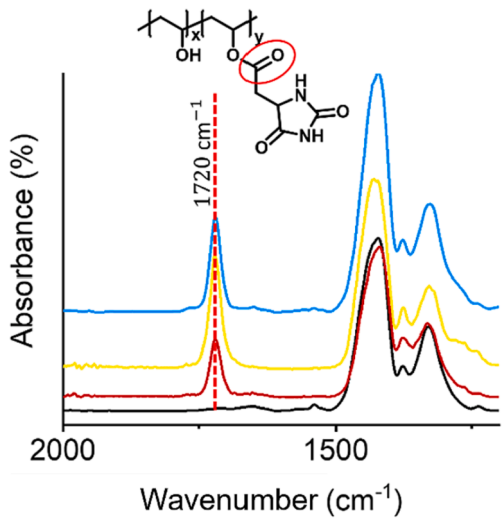

Fig. 2. Detail of the FT-IR spectra acquired on washed and freeze-dried samples of, from bottom to top, non-functionalized H-PVA gel (black), H-PVA-hyd gel (red), H-PVA-hyd/L-PVA gel (yellow), and H-PVA-hyd/starch gel (light blue). The presence of a peak centered at 1720 cm^{-1} relative to C═O stretching modes is related to the permanence of the hydantoin functionality in the cryogel samples upon 1 week of washing in ultrapure water. (For interpretation of the references to color in this figure legend, the reader is referred to the web version of this article.)

spectroscopy. The formation of *N*—Cl groups was confirmed following spectral changes in the 1800–1600 cm^{-1} region, relative to C═O vibrational modes of ester, imide, and amide groups, [31] and/or the appearance of new peaks below 1000 cm^{-1} (*N*—Cl vibrational modes [32]). Freeze-dried samples were also redissolved in deuterated DMSO-d_6 and analyzed by ^{1}H NMR. In this case, we followed signals at 5.14 ppm (relative to the ethanic hydrogen of H-PVA), 7.86 ppm (relative to the proton of the hydantoin imide group), and 10.70 ppm (relative to the proton of the hydantoin amide group).

2.9. Biological tests

The antimicrobial activity of the hydrogels was investigated against the model Gram-positive bacteria *Bacillus subtilis (B. subtilis)* by "agar diffusion test" [33] and "viability test" [34]. The bacterial pellet was reactivated in tryptic soy broth (TSB) at 32 °C and overnight agitation at 260 rpm. The obtained bacterial dispersion was diluted in fresh TSB to the optical density of 1, measured by Thermo Scientific NanoDrop OneC UV–Vis Spectrophotometer at 600 nm of wavelength (OD_{600}), and stored at −20 °C by the addition of 25 wt% of sterile glycerol.

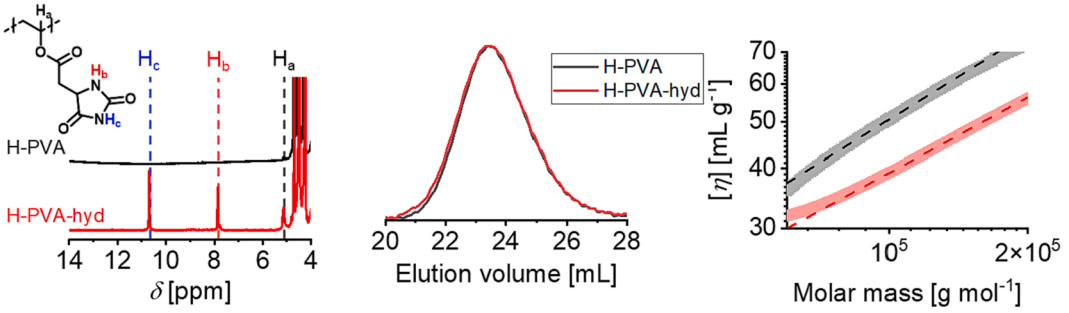

Fig. 1. Experimental insights on the functionalization of H-PVA with hydantoin-5-acetic acid resulting in H-PVA-hyd. **Left**: overlay of the ^{1}H NMR spectra of H-PVA and H-PVAhyd in the region between 4.0 and 14.0 ppm and schematic interpretation of the signals. **Middle**: Size exclusion chromatography (*SEC*) chromatograms before and after functionalization from the refractive index detector. **Right**: Logarithmic plot of the intrinsic viscosity over molar masses (before and after functionalization). The dotted lines represent experimental data. The shaded lines correspond to the linear fitting employed for the calculation of Mark-Houwink constants k and α (see equation (2)).

Table 2
Summary of the quantitative analysis performed via ^{1}H NMR on the functionalized gels to determine the permanence of hydantoin functionality after washing the samples in ultrapure water for 1 week. (%mol refers to the molar ratio between non-modified and functionalized H-PVA monomers). All the results are reported as mean values of three repetitions.

Gel sample	Hydantoin unwashed gels (%mol)	Hydantoin after washing (%mol)	Hydantoin after washing (%)
H-PVA-hyd	1.61 ± 0.11	1.12 ± 0.05	68.2
H-PVA-hyd/L-PVA	1.22 ± 0.07	1.29 ± 0.04	> 99
H-PVA-hyd/Starch	1.43 ± 0.09	1.19 ± 0.05	82.3

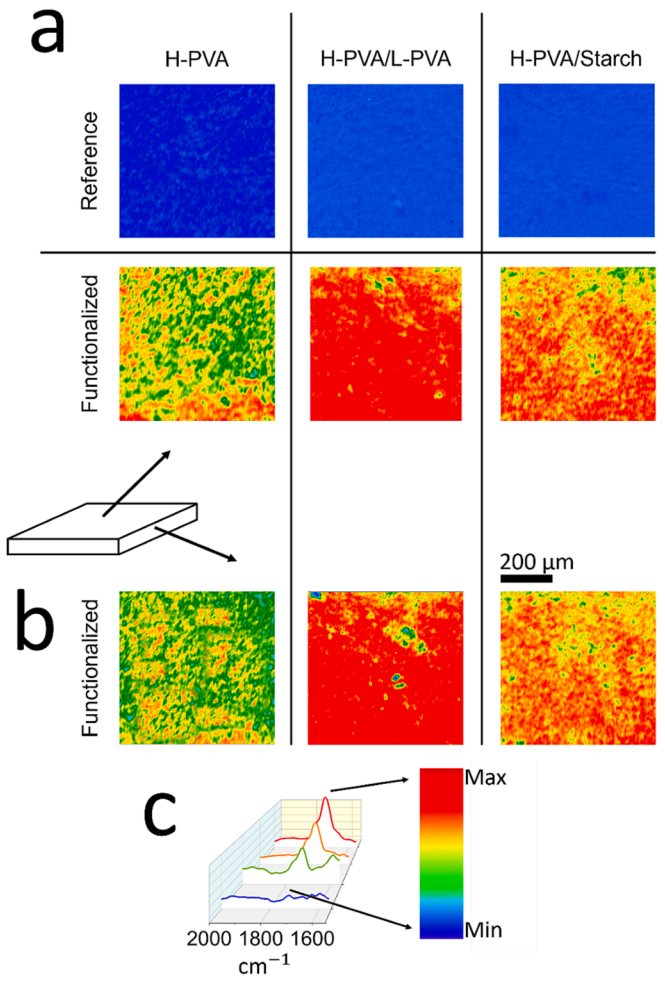

Fig. 3. Results of the µFT-IR mapping performed on non-functionalized H-PVA, H-PVA/L-PVA, and H-PVA/starch cryogels, and on their hydantoin-containing counterparts (H-PVA-hyd, H-PVA-hyd/L-PVA, and H-PVA-hyd/starch). The presence of the hydantoin functionalization and its spatial distribution in the gels' volume was assessed by integrating the relative intensity of the IR signal centered at 1720 cm^{-1}, relative to the stretching vibrational modes of the C═O of carbonyl, amide, and imide groups of the hydantoin substituent [43].

2.9.1. *Agar diffusion test*

In order to estimate the antibacterial activity, we first performed the "agar diffusion test" by inoculation of 5 µL of bacterial suspension in a tryptic soy agar plate (TSA). Then hydrogel samples of 0.5 × 0.5 × 0.2 cm^3 were placed on the inoculated surface and incubated at 32 °C monitoring the inhibition zone and the biological effects after 24 h.

2.9.2. *"Viability test"*

The viability and proliferation of the bacterial cells after the exposition to the functionalized gels were also tested by the LIVE/DEAD BacLight™ (Thermo Fisher Scientific) Kit assay [35,36]. The BacLight Kit is constituted of the two nucleic acid-binding stains SYTO9 and propidium iodide (PI) which can selectively highlight the safe and damaged bacterial cells. SYTO9 dye can penetrate all the bacterial membranes, giving the cell the characteristic fluorescence at 488 nm, while the PI can only penetrate the damaged membranes with the resulting emission wavelength of 636 nm. The dye solutions as received were diluted to the final concentration of 3.34 µM and 20 µM, respectively SYTO9 and PI, in a sterile solution of 10 wt% of NaCl. The hydrogels removed from the inoculated surface were gently placed in an 8-well Labtec® sterile plate with 100 µL of the fluorescent probes and equilibrated in dark under low agitation for 30 min. The viability of the *B.subtilis* was then evaluated by direct observation through CLSM. The stack images of 146.22 × 146.22 μm^2 were acquired with the instrument setup previously detailed in section 2.4. To correctly resolve touching cells and acquire the correct population of live and dead cells, micrographies were binarized and processed through the Watershed and 3D Objects Counter methods of ImageJ [37]. This second plugin is a collection of mathematical methods that allow the determination of bi-dimensional and three-dimensional objects in a collected stack, counting each detected object and generating a false color map where each object is highlighted in a different color and serial number to immediately detect possible bias due to the image data process. The prepared systems were tested in triplicate and at least five different portions of each system were investigated in the viability test by CLSM.

3. Results and discussion

Aiming to develop novel PVA-based cryogels featuring antimicrobial activity, the reaction of functionalization of a poly(vinyl alcohol) (H-PVA) featuring a high degree of hydrolysis (>99 %) was performed with hydantoin-5-acetic acid. To this end, a low vinyl alcohol (meric structure of PVA) to hydantoin ratio of 4 mol% was tested. Briefly, a two-step reaction was performed comprising (a) the activation of hydantoin-5-acetic acid with carbonyl diimidazole and (b) the formation of the PVA-hydantoin ester linkages (see scheme 1). ^{1}H NMR analysis of the purified product, PVA-hyd, revealed the presence of all the signals related to H-PVA (full spectra reported in SI, Figure S2). Moreover, the functionalization with hydantoin-5-acetic acid resulted in the imide and amide signals of the heterocycle (10.7 and 7.9 ppm in DMSO-d_6, respectively), while a new peak related to the methine hydrogen of the hydantoin ester unit at 5.14 ppm (proton labeled as B2 in Figure S2 in SI) was detected. As a result, the successful functionalization reaction was verified, and the new ester-related signal was employed for the calculation of the substitution degree according to equation (1):

$$f_{exp}(mol\%) = 100 \bullet \frac{I_{B2}}{I_{B2} + I_{B1}} \quad (1)$$

where f_{exp} is the functionalization percentage expressed in mol, and I_{B1} and I_{B2} are the integrated areas of the ^{1}H NMR peaks relative to the protons B_1 and B_2 (see Figure S2 in SI), respectively. As a result, a f_{exp} of 3.5 % was calculated and corresponded to a conversion of 86.4 % in excellent agreement with the overall yield of 86.5 %.

Additionally, insights were accessed via the estimation of blockiness and average chain length of both hydantoin- and alcohol-containing blocks of the functionalized PVA according to a literature procedure [38–40]. The calculation resulted in a blockiness value of 0.67

Table 3
Summary of the viscoelastic behavior of functionalized samples (cryogels containing the newly synthesized H-PVA-hyd polymer) and of their non-functionalized counterparts. All the gels are characterized by viscoelastic responses that classify them as "strong gels". All the results are reported as mean values of three repetitions.

	H-PVA (1FT)	H-PVA-hyd (2FT)	H-PVA/L-PVA (1FT)	H-PVA-hyd/L-PVA (2FT)	H-PVA/starch (1FT)	H-PVA-hyd/starch (2FT)
G′	575.25	578.98	1037.22	405.39	1017.43	2734.28
(Pa)	±50.61	±25.29	±165.17	±58.67	±198.77	±55.19
G″	22.75	25.01	72.80	21.61	74.14	134.91
(Pa)	±6.62	±2.99	±24.13	±1.43	±29.75	±5.30

suggesting a tendency to statistically distributed vinyl hydantoin meric units (pure block 0.0, statistical copolymers 1.0) with a statistical average spacing of around 75 vinyl alcohol units.

Given the quasi-statistical distribution of hydantoin moieties, one could expect a variation in the physicochemical properties of the PVA-hyd in comparison with the starting H-PVA. In this regard, even a low functionalization of the PVA could result in the variation of solubility features, affecting the dynamics of the freeze-thawing process used for hydrogel preparation. Insights on the solubility features were assessed by means of *SEC* analysis in water eluent employing a triple-detection system (multi-angle light scattering (MALS), viscosimeter (Visco), refractive index (RI) detection). The results of these measurements are summarized in Fig. 1. The analysis of PVA before and after functionalization revealed a complete superimposition of the RI traces, while the specific viscosity chromatograms featured a similar shape, but a lower peak area for PVA-hyd, suggesting a variation in the conformational features. The determination of molar masses was assessed employing both MALS-RI and Visco-RI (volumetric calibration) methodologies. Both methods resulted in a similar number-average molar mass of around 115 kg mol^{-1} for both the starting and the functionalized PVA, while a broad dispersion of molar masses (Đ) of around 1.45 for MALS-RI and above 2.60 for Visco-RI approaches were found. Despite the similar molar masses, the slight variation in the chromatogram intensities from specific viscosity, which is directly connected to intrinsic viscosity, suggested the variation of conformational features of the functionalized PVA and, therefore, also a variation of polymer-water interaction. The estimation of such feature was accessed employing the Mark-Houwink equation (MH, equation (2).

$$[\eta] = kM^{\alpha} \quad (2)$$

Where $[\eta]$ is the intrinsic viscosity of the polymer in the selected solvent at a given temperature, M is the molar mass, and k and α are the MH parameters that are related to polymer–solvent interactions. Similarly to literature data, the parameter α of MH for PVA resulted in a value of 0.59 and a k value of 0.051 mL g^{-1} that are typically found for polymers in good solvents [41,42]. Already a low functionalization degree of 3.5 % with hydantoin esters resulted in a decrease of the parameter α down to 0.51 (close to theta conditions, $\alpha = 0.50$) while the parameter k almost doubled after functionalization ($k = 0.093$ mL g^{-1}). The results revealed that the functionalization resulted in a contraction of the polymer chain already in diluted solutions and hinted toward the variation of solubility features that are connected to the freeze-thawing dynamics during cryogel preparation. Aiming to access a new class of PVA cryogels featuring an effective biocidal activity, the increase of functionalization degree is of interest to add moieties that can serve, upon activation, as biocidal. However, the close value of the α parameter of PVA-hyd to the theta condition, which represents a threshold for the polymer solubility, suggested its direct application for the formulation of biocidal hydrogels.

Gel samples containing H-PVA-hyd polymer were prepared as described in the Materials and Methods section, and their compositions are summarized in Table 1. Afterward, the gels were placed in milli-Q water to equilibrate. During this process, two main phenomena occur which are the swelling of the gel network, due to an increase in the water content of the gel, and the leaving of polymeric portions of the gel that are not stably linked to the newly formed three-dimensional network (i.e., gels obtained via freeze-thawing always display a gel content lower than 100 %). Therefore, if on one hand the freeze-thawing method allows avoiding the use of organic solvents, catalyzers, and crosslinkers, on the other it can result in the loss of functionalized polymeric chains in the final gel. The permanence of functionalization in the systems was hence verified via FTIR-ATR experiments on freeze-dried samples. The acquired spectra, a detail of which is shown in Fig. 2 (full spectra of all the samples, including "blank" H-PVA/L-PVA and H-PVA/Starch, are reported in SI, Figures S3-S5.), are characterized by the clear presence of a peak at 1720 cm^{-1}, which was attributed to the stretching mode of the esteric C═O group [43] highlighted in Fig. 2. Peaks relative to amide and imide C═O are reported to arise in the same spectral range [44] and are here assumed to contribute to the overall observed signal.

The permanence of the functionalization was further assessed via ^{1}H NMR. In this case, it was also possible to quantitatively determine the percentage of functionalized monomers in the gels (with respect to the non-functionalized ones, carrying the original –OH group), which resulted higher than 99 % for the H-PVA-hyd/L-PVA gel (values summarized in Table 2). ^{1}H NMR spectra and the formulae used for calculating the molar ratio of the functionalized monomers are reported in detail in SI (section S4, Figures S6-S8).

As noticeable, the higher percentages are relative to H-PVA-hyd/L-PVA and H-PVA-hyd/Starch gels, which are the samples in whose formulation a component known to be immiscible (or poorly miscible) with H-PVA is present. It is known from the literature that H-PVA/L-PVA and H-PVA/Starch mixtures in water show prominent phase separation [25,26], where the continuous phase is formed by H-PVA, while the discontinuous phase is rich in the second polymeric component. Hence, considering that the phase separation causes an increment in the effective concentration of the component in the continuous phase (H-PVA) and that this process leads to the formation of denser networks with higher crystallinity [25,26,45], it is reasonable to assume that the functionalized PVA (H-PVA-hyd) is more efficiently retained in the H-PVA network and/or participates more in the direct formation of crystalline nodes in the gel network [25]. Based on these observations, we can conclude that even if H-PVA-hyd shows slightly different behavior in water than unfunctionalized H-PVA (as determined via *SEC*-MALS measurements and the Mark-Houwink equation), it remains largely miscible with the latter and does not significantly enter in the composition of the discontinuous phase in the pre-gel solutions. The chosen strategy to introduce a non-miscible (or poorly miscible, porogen) polymer in the system to promote the permanence of the functionalized polymer in the network was successful.

Freeze-dried gel samples were also analyzed by using μFT-IR mapping, to follow the spatial distribution of the hydantoin functionality. μFT-IR maps were acquired both on the transversal and longitudinal sections of the samples. The obtained FT-IR maps are reported in Fig. 3. The hydantoin functionality is homogeneously distributed in all three samples, and the semiquantitative analysis confirms the relative hierarchy of the molar H-PVA/H-PVA-hyd ratios calculated from ^{1}H NMR experiments (H-PVA-hyd < H-PVA-hyd/Starch < H-PVA-hyd/L-PVA).

The viscoelastic behavior of the H-PVA-hyd-containing samples was investigated via rheological experiments. The rheological characterization of both the reference samples and the modified ones revealed that

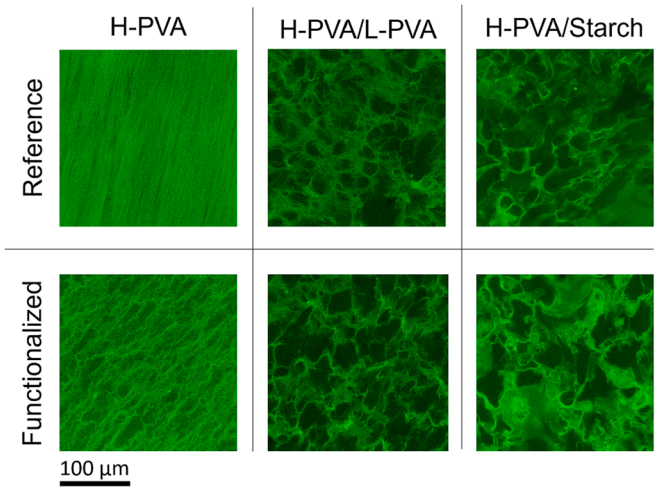

Fig. 4. 2D imaging of cryogel samples swollen in Rhodamine 110 solutions acquired via CLSM. Upper row, from left to right: H-PVA, H-PVA/L-PVA, and H-PVA/starch gels. Bottom row, from left to right: H-PVA-hyd, H-PVA-hyd/L-PVA, and H-PVA-hyd/starch gels.

the two series of samples are characterized by comparable viscoelastic properties and are all classifiable as strong gels, based on the values of their storage (G′) and loss (G″) moduli [42], which values are summarized in Table 3 (1 % oscillation strain fixed, frequency sweep mode, data presented as recorded at 1 Hz). Detailed results of the rheological measurements and their discussion are reported in SI (Figures S9 and S10).

The gels' morphology was investigated via CLSM imaging. As reported in Fig. 4, all three samples containing H-PVA-hyd are characterized by a sponge-like structure (three-dimensional images of the samples were also acquired and are reported in SI, Figure S11), with pores' diameters ranging from 7 to 20 μm, as calculated through MorpholibJ/ImageJ analysis (details reported in section 2.4, results reported in SI, section S8). This morphology is not random, but it is formed as a consequence of mixing poorly miscible polymers in the pre-gel solutions, resulting from the so-triggered phase separation events. We underline, however, that contrarily to samples H-PVA-hyd/L-PVA and H-PVA-hyd/Starch, H-PVA-hyd does not follow the pattern observed in its non-functionalized homolog. Indeed, H-PVA gels obtained via freeze-thawing are characterized by a rather compact structure, displaying tight elongated pores following parallel directions, with pores diameters of approximately 4 μm [29]. H-PVA-hyd gel, on the contrary, shows a different porous pattern, which suggests that some phase separation occurred prior to freeze-thawing, involving the functionalized blocks of the H-PVA-hyd chains [25,46]. The samples containing a phase-separating component (i.e., L-PVA or starch) show pores with diameters up to 20 μm, which is an interesting feature from an applicative perspective. The biocidal functionalities are in fact present not only on the outer surface of the gels (i.e., the gel portion that would be in direct contact with a surface to treat such as a wound) but are evenly distributed also in the inner part of the systems (as assessed via μFT-IR mapping, see Fig. 3). Therefore, to maximize the biocidal action, the journey of bacteria inside the gel matrix (both via passive and active movement) must be allowed from a dimensional point of view. In this contribution, we tested the efficacy of the systems towards *B.subtilis*, which have a size of approximately 4−10 × 0.25−1 μm: hence dimensionally compatible with the gels.

In order to activate the hydantoin groups (through the formation of *N*—Cl bonds), the functionalized gel samples have been immersed in a 10 % NaClO solution for 30 s. This protocol was chosen after preliminary tests subjecting the samples to a longer immersion time, since immersions lasting from several minutes to hours are often described in the literature for halamine-containing materials [47,48] and lower NaClO concentration (1 %). However, the tested conditions yielded weaker gels with no hydantoin detected after treatment (see SI for full discussion). It is known that the oxidative power of NaClO can affect the integrity of the PVA chains [49], possibly causing their breakage also in proximity of the functionalized points, which in our case resulted in loss of hydantoin functionality. The treatment at higher concentrations of NaClO and for a shorter time resulted in gels maintaining of the mechanical properties (see Figure S14 in SI) as well as the permanence of the hydantoin functionality (see ^{1}HNMR analysis, Figure S15 in SI).

The effectiveness of the chlorination process (i.e., of the formation of the *N*—Cl bond) was first assessed via FTIR-ATR experiments (spectra reported in SI, Figures S14-S15). It is known from the literature that the formation of the *N*—Cl group causes a decrease in the intensity of a peak around 3200 cm^{-1} relative to the N—H stretching modes [32,43], the shift of the peaks relative to the C═O of the amide and imide groups (in the 1800–1500 cm^{-1} spectral range), and the appearance of signals at wavenumbers values below 1000 cm^{-1} [32]. The first spectral feature is usually the most evident, but in our case, the N—H stretching peak is hidden due to the presence of a broad peak centered at around 3300 cm^{-1}, typical of the –OH stretching of PVA [50]. Nevertheless, a shift of the overall signal (from 3300 3250 cm^{-1}, see Figures S13-S15 in SI) in the spectral area of interest suggests that changes regarding the N—H stretching band may have occurred. A shift of the C═O signal was observed in all the samples, while the appearance of a peak below 1000 cm^{-1} was clearly visible only for samples H-PVA-hyd and H-PVA-hyd/L-

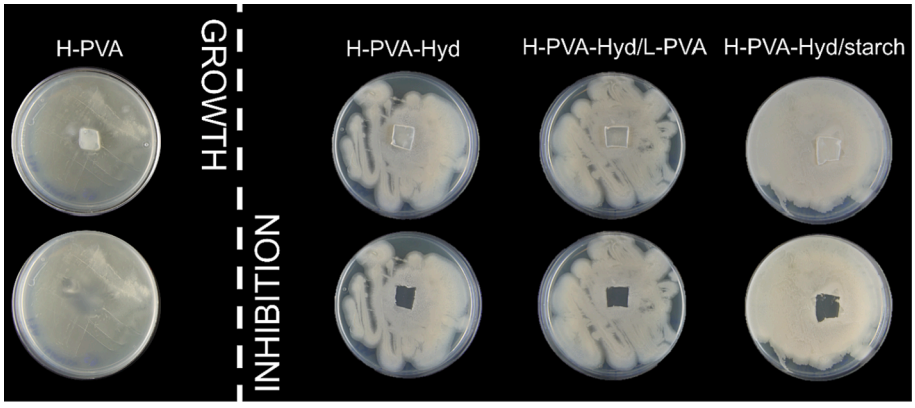

Fig. 5. Pictures of TSA solid media inoculated with *B.subtilis* and incubated at 32 °C for 24 h. The activated (chlorinated) gel samples were placed on top of the solid media after inoculation and before incubation. Upper row: appearance of the hydantoin-containing gels and of a H-PVA reference gel on the bacterial culture after 24 h of incubation. Bottom row: appearance of the inoculated solid media after the gels' removal. As noticeable, the reference H-PVA gel did not affect the bacterial growth in the contact zone. On the contrary, all the hydantoin-containing samples left a clean surface under them.

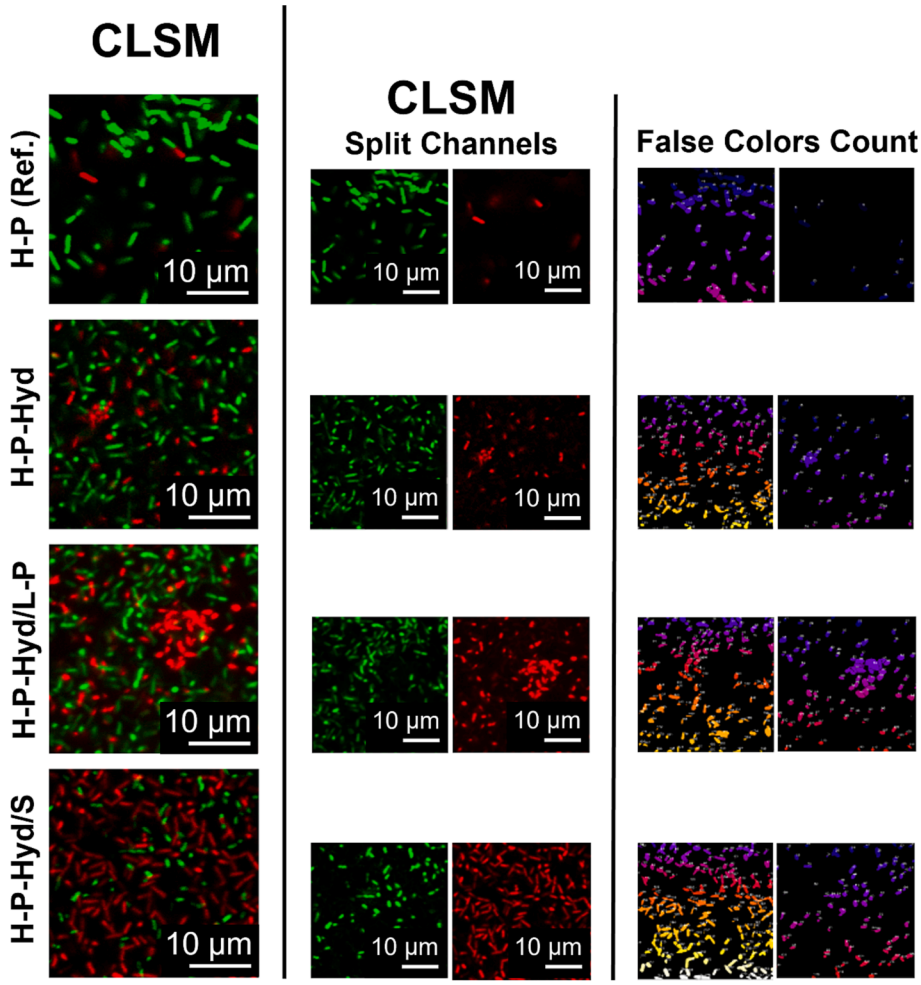

Fig. 6. Micrographies of the live/dead bacteria cells that migrated from the solid *B.subtilis* culture inside the gel samples. The images of the samples were acquired via confocal laser scanning microscopy (CLSM) after treatment with the LIVE/DEAD BacLight™ kit. The split channels (middle column) highlight the live (green cells) and the damaged or dead bacteria (red cells). In the right column, the corresponding reconstructed images are reported. These false color images have been obtained and processed via the Watershed and 3D Objects counter methods of ImageJ, as described in section 2.9.2 ("Viability test"). (For interpretation of the references to color in this figure legend, the reader is referred to the web version of this article.)

PVA. In the H-PVA-hyd/Starch sample, the signal is less identifiable due to the abundance of signals characteristic of starch itself in the same range. Hence, to assess the effectiveness of the chlorination for the the H-PVA-hyd/Starch sample (and to confirm the chlorination of the H-PVA-hyd and H-PVA-hyd/L-PVA samples), ^{1}H NMR spectra of samples treated with NaClO were collected and a detail of the results is reported in SI - Figure S18. In all the samples no signals at 10.8 ppm (N—H amide proton, see spectra in Fig. 1 for reference) were detected, while in sample H-PVA-hyd/Cl a small peak around 10 ppm appeared. This evidence suggests that in H-PVA-hyd/L-PVA/Cl and H-PVA-hyd/starch/Cl, the protons linked to the amide nitrogen are substituted by chlorine, while for H-PVA-hyd/Cl some amide groups are still intact, but the signal of the N—H proton is shifted due to changes in the chemical environment. Similarly, the signal originally at around 7.9 ppm and relative to the imide group (see Fig. 1 for reference) is shifted in all spectra (as a consequence of the chlorination of the neighboring amide nitrogen), suggesting that the chlorination of this group is less likely to occur.

The biological effects of the activated gels were evaluated by direct application of the samples to the inoculated TSA solid media and compared to a reference H-PVA gel (*i.e.*, a H-PVA gel that underwent the same NaClO treatment followed by 48 h of washing in ultrapure water as the H-PVA-hyd containing samples). After 24 h of incubation, the gels were removed, and the inoculated solid media was observed. Fig. 5 shows that the H-PVA reference gel did not affect bacterial colonization, while hydantoin-functionalized hydrogels successfully inhibit bacterial growth on the whole contact area. Furthermore, no inhibition rings were formed around the gel samples, indicating that the inhibition effect is restricted to the area directly in contact with the functionalized hydrogel and no undesired release of antimicrobial functionality has occurred.

These preliminary results support the excellent spatial control of the biocidal effect of these functionalized gels. Moreover, this observation suggests that the predominant mechanism of inactivation and killing involves, at some stage, the direct contact of the *N*—Cl group with the bacterial target as suggested by Natan et al. [51], rather than the release of free oxidative chlorine in the media.

After 24-hour contact with the inoculated media, the hydantoin-containing gel samples were carefully moved into a microscopy sample holder and treated with the LIVE/DEAD BacLight™ kit as described in section 2.9.2. The in vitro biocidal efficiency of the hydrogel samples applied to the inoculated surface was quantitatively assessed by CLSM. Thanks to the selective labeling of the bacteria cells by the fluorescent probes (SYTO9 and PI) live and damaged bacterial cells were observed (see Fig. 6), and the corresponding population distributions were determined by the ImageJ data process. 2D micrographies show (Fig. 6) the hydantoin-active hydrogels expose a population of damaged bacteria cells (red channel) significantly higher than the equivalent inactivated gel.

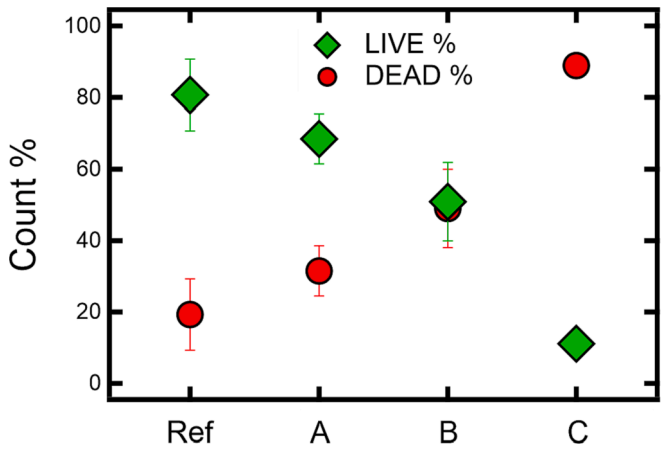

Fig. 7. Normalized population of the live/dead bacterial cells determined by the vitality test conducted on the gel samples after 24 h of incubation on solid TBS media inoculated with *B.subtilis*. Calculations were performed via image analysis by means of the Watershed and 3D Objects counter methods of ImageJ, as described in section 2.9.2 ("Viability test"). Ref: H-PVA gel, A: H-PVA-hyd gel, B: H-PVA-hyd/L-PVA gel, C: H-PVA-hyd/starch gel.

The live and dead bacteria cells were determined by splitting the green and red channels from the original 2D images. The resulting live/dead populations reported in Fig. 7 highlight the biocidal effect of the functionalized gels, which expose a significant increase in bacterial mortality with the highest value of ≈ 90 % in the case of the H-PVA-hyd/starch gel. These results confirm the preliminary data obtained from plate culture, identifying a significant reduction in bacterial proliferation on the applied surfaces and confirming the almost un-effected biological activity by the not activated functionality.

Interestingly, the efficacy of bacterial suppression performed by the hydantoin-containing gels did not follow the hierarchy of mol/mol% functionality calculated via ^{1}H NMR on washed gels (i.e. H-PVA-hyd < H-PVA-hyd/starch < H-PVA-hyd/L-PVA, see Table 2 and supporting Figures S6-S8 in SI), being H-PVA-hyd/starch the most effective. This behavior could be explained either by assuming that in the said system the activation (chlorination) of the hydantoin groups was more effective or that the presence of organic matter in the network (starch is an available food source for *B.subtilis* [52]) enhanced the bacterial mobility via chemotactic mechanisms [53], incrementing the statistical probability of bacteria-hydantoin contacts and consequent inactivation/killing. The latter hypothesis is supported by calculations on the total number of bacteria in the gels, as obtained by analyzing 15 portions of separate gel samples for each system and normalizing the values on a gel volume of 150x150x25 μm^3. The overall bacterial population (live and dead cells) follows the order H-PVA-hyd < H-PVA-hyd/L-PVA < H-PVA-hyd/starch (data reported in SI, Table S1), indicating that the entity of migration of the bacterial cell from the plate culture to the inside of the network is system-dependent. However, while the lowest number of cells in H-PVA-hyd can be explained by considering the sensibly lower dimensions of its pores (maximum diameter 7 μm) compared to both H-PVA-hyd/L-PVA and H-PVA-hyd/starch (maximum diameter 20 μm, as discussed earlier and reported in SI), considerations on pores dimensions are not sufficient to justify the difference in bacterial population between H-PVA-hyd/L-PVA and H-PVA-hyd/starch.

The two systems show similar morphologies (see Fig. 4) and the same pore dimensions (see SI, section S8), indicating that additional factors, such as the presence of a biopolymer in the structure, have to be considered. Indeed, even if in H-PVA-hyd/starch starch was introduced as a phase-segregating component, its permanence in the final gel is high even after swelling, as previously reported [26] and confirmed here by ^{1}H NMR analysis (see Figure S8 in SI). However, a simple iodine reaction performed on a 3x3 cm^2 gel sample evidenced its inhomogeneous distribution at the *meso*-scale (see Figure S19 in SI). Hence, if chemotactic mechanisms influencing bacterial motility are involved, a similar inhomogeneity in the distribution of the bacterial population inside the gel should be observed.

Evidence of inhomogeneous distribution of bacterial population inside the starch-containing gels was observed in the CLSM collected images of different samples. The images reported in Fig. 8 (panel 2, images a, b, and d) highlight the presence of a non-random distribution pattern in starch-containing samples (for a 360 °C view of the samples, a video is provided in the "Supplementary Material" section), as opposed to the homogeneous spreading of bacterial cells inside the matrix of the starch-free samples (Fig. 8, panel 1, images A and B). Moreover, transversal sections obtained from the 3D imaging of starch-containing samples (Fig. 8, panel 2, image d) highlight an interesting analogy between the bacterial distribution pattern and the morphology of the H-PVA-hyd/starch gel in which they are contained (see Fig. 8, panel 2, image e), further supporting the hypothesis of a chemo-specific attraction of the bacteria towards the gel. These findings are in support of a chemotactic

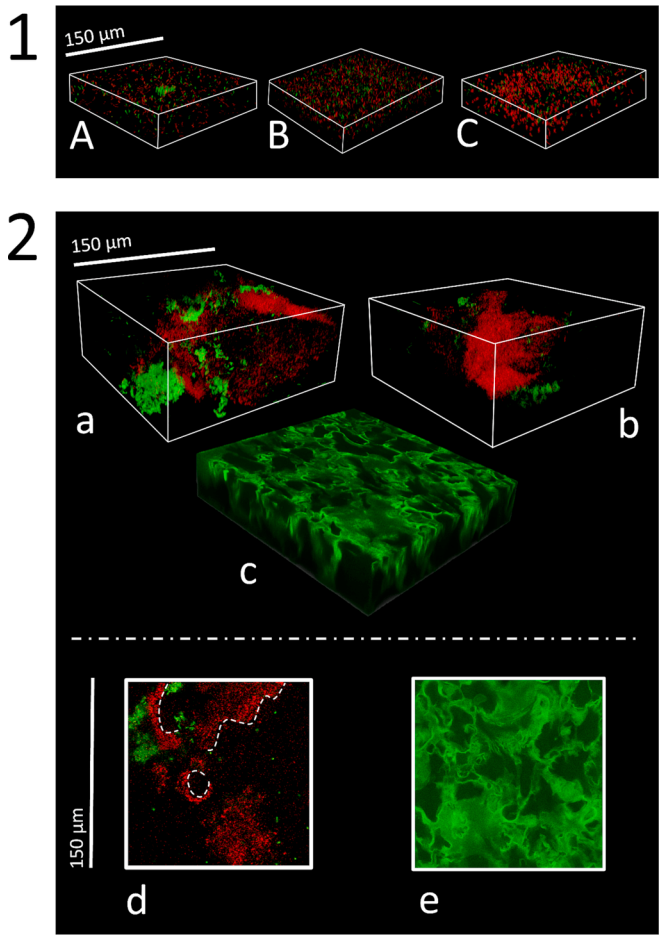

Fig. 8. Distribution of the bacterial (*B. Subtilis*) population inside the gels containing activated hydantoin, as observed via CLSM experiments and after staining the bacterial cells with the LIVE/DEAD BacLight™ kit. Random spreading of the bacteria was observed in all the investigated areas for H-PVA-hyd (panel 1, image A), and H-PVA-hyd/L-PVA gels (panel 1, image B). For the H-PVA-hyd/starch system, both random (panel 1, image C) and patterned inhomogeneous (panel 2, image a, b, and d) bacterial distributions were observed. Transversal sections of bacterial imaging performed on starch-containing samples (Fig. 8, panel 2, image d) highlight an interesting analogy between the bacterial distribution pattern and the morphology of the H-PVA-hyd/starch gel in which they are contained (see Fig. 8, panel 2, images c and e), further supporting the hypothesis of a chemo-specific attraction of the bacteria towards the gel.

mechanism involved in the outstanding biocidal efficacy shown by the H-PVA-hyd/starch systems. Further research will be performed to understand the influence of a bioavailable food source embedded in a complex porous network on the bacterial motility of different strains.

4. Conclusions

A novel biocidal PVA-hydantoin polymer (H-PVA-hyd) was successfully synthesized via an esterification reaction and employed for the formulation of highly efficient antibacterial cryogels. To further enhance the antimicrobial potential of these systems, we implemented a "Trojan Horse" strategy by embedding a polymeric bacterial nutrient source (starch) within the H-PVA-hyd-based network. We conducted biocidal efficacy assessments on different H-PVA-hyd cryogels, both with and without starch, employing model bacteria with amylolytic activity (*Bacillus subtilis*). Our findings demonstrated the remarkably superior effectiveness of the starch-containing systems. As hypothesized, starch serves a dual role in the system: it acts as a stabilizer for the cryogels and enhances their biocidal efficacy. Indeed, the phase-separation processes observed in the H-PVA-hyd/starch gels result in a more efficient incorporation of the biocidal polymer within the cryogel matrix.

Furthermore, starch promotes bacterial migration within the gel (reasonably due to chemotactic attraction), consequently increasing their contact rate with the activated biocidal groups within the gel matrix. The overall process leads to an impressive bacterial killing rate of 90 %. The outstanding biocidal power of these gels, coupled with their appealing viscoelastic features makes them promising candidates for advanced wound dressing applications.

While simple PVA-based cryogels have already been established as ideal materials for this purpose in terms of mechanical properties and water content [5], our systems represent a crucial step forward in terms of antibacterial protection. Indeed, they overcome the drawbacks of simply dispersing antibiotics [8,14] or oxidizing agents [10,17] in the gel matrix by carrying a rechargeable and highly selective biocidal functionality (hydantoin) directly linked to the polymeric scaffold. The demonstrated effectiveness of H-PVA-hyd/starch gels towards amylolytic bacteria such as *B. subtilis* suggests the exciting potential to customize highly biocidal cryogels for specific bacteria groups based on their enzymatic activity. This can be achieved by varying the polymeric chemoattractant within the gel matrix. Our future research will explore this hypothesis by incorporating proteic and lipidic components into H-PVA-hyd-based gel networks, which will be evaluated against bacteria with proteolytic and lipolytic activity.

CRediT authorship contribution statement

Vanessa Rosciardi: Conceptualization, Investigation, Data curation, Validation, Writing – original draft. **Damiano Bandelli:** Methodology, Investigation, Data curation, Writing – original draft. **Gavino Bassu:** Methodology, Investigation, Writing – original draft. **Ilaria Casu:** Investigation. **Piero Baglioni:** Conceptualization, Project administration, Supervision, Validation.

Declaration of competing interest

The authors declare that they have no known competing financial interests or personal relationships that could have appeared to influence the work reported in this paper.

Data availability

Data will be made available on request.

Acknowledgments

This project has received fundings from CSGI (Consorzio per lo Sviluppo dei Sistemi a Grande Interfase, Center for Colloid and Surface Science) and from the European project GREENART (GREen ENdeavor in Art ResToration) under the Horizon Europe Grant Agreement 101060941. Views and opinions expressed are however those of the author(s) only and do not necessarily reflect those of the European Union or the European Research Executive Agency (REA). Neither the European Union nor the granting authority can be held responsible for them.The authors are grateful to Silvia Tilli for her support and supervision in biological laboratory practices.

Appendix A. Supplementary data

Supplementary data to this article can be found online at https://doi.org/10.1016/j.jcis.2023.11.142.

References

[1] S. Morariu, M. Bercea, L.M. Gradinaru, I. Rosca, M. Avadanei, Versatile Poly(Vinyl Alcohol)/Clay Physical Hydrogels with Tailorable Structure as Potential Candidates for Wound Healing Applications, Mater. Sci. Eng. C (2020) 109, https://doi.org/10.1016/J.MSEC.2019.110395.
[2] S. Jiang, S. Liu, W. Feng, PVA Hydrogel Properties for Biomedical Application, J. Mech. Behav. Biomed. Mater. 4 (7) (2011) 1228–1233, https://doi.org/10.1016/J.JMBBM.2011.04.005.
[3] M. Razavi, Y. Qiao, A.S. Thakor, Three-Dimensional Cryogels for Biomedical Applications, J. Biomed. Mater. Res. A 107 (12) (2019) 2736–2755, https://doi.org/10.1002/JBM.A.36777.
[4] C.M. Hassan, N.A. Peppas, Structure and Applications of Poly(Vinyl Alcohol) Hydrogels Produced by Conventional Crosslinking or by Freezing/Thawing Methods, Adv. Polym. Sci. 153 (2000) 37–65, https://doi.org/10.1007/3-540-46414-X_2/COVER.
[5] E.A. Kamoun, E.R.S. Kenawy, X. Chen, A Review on Polymeric Hydrogel Membranes for Wound Dressing Applications: PVA-Based Hydrogel Dressings, J. Adv. Res. 8 (3) (2017) 217–233, https://doi.org/10.1016/J.JARE.2017.01.005.
[6] J.S. Chin, L. Madden, S.Y. Chew, D.L. Becker, Drug Therapies and Delivery Mechanisms to Treat Perturbed Skin Wound Healing, Adv. Drug. Deliv. Rev. 149–150 (2019) 2–18, https://doi.org/10.1016/J.ADDR.2019.03.006.
[7] A. Górska, A. Krupa, D. Majda, P. Kulinowski, M. Kurek, W.P. Węglarz, R. Jachowicz, Poly(Vinyl Alcohol) Cryogel Membranes Loaded with Resveratrol as Potential Active Wound Dressings, AAPS Pharm. Sci. Tech. 22 (3) (2021) 1–14, https://doi.org/10.1208/S12249-021-01976-1/TABLES/4.
[8] L. Rosselle, A.R. Cantelmo, A. Barras, N. Skandrani, M. Pastore, D. Aydin, L. Chambre, R. Sanyal, A. Sanyal, R. Boukherroub, S. Szunerits, An 'on-Demand' Photothermal Antibiotic Release Cryogel Patch: Evaluation of Efficacy on an Ex Vivo Model for Skin Wound Infection, Biomater. Sci. 8 (21) (2020) 5911–5919, https://doi.org/10.1039/D0BM01535K.
[9] Y.N. Martínez, I. Cavello, R. Hours, S. Cavalitto, G.R. Castro, Immobilized Keratinase and Enrofloxacin Loaded on Pectin PVA Cryogel Patches for Antimicrobial Treatment, Bioresour. Technol. 145 (2013) 280–284, https://doi.org/10.1016/J.BIORTECH.2013.02.063.
[10] T.J. Smith, J.E. Kennedy, C.L. Higginbotham, The Rheological and Thermal Characteristics of Freeze-Thawed Hydrogels Containing Hydrogen Peroxide for Potential Wound Healing Applications, J. Mech. Behav. Biomed. Mater. 2 (3) (2009) 264–271, https://doi.org/10.1016/J.JMBBM.2008.10.003.
[11] E.C. Murphy, A.J. Friedman, Hydrogen Peroxide and Cutaneous Biology: Translational Applications, Benefits, and Risks, J. Am. Acad. Dermatol. 81 (6) (2019) 1379–1386, https://doi.org/10.1016/J.JAAD.2019.05.030.
[12] J. Crew, R. Varilla, T.A. Rocas, D. Debabov, L. Wang, A. Najafi, S.A. Rani, R. Najafi, (Ron); Anderson, M., NeutroPhase® in Chronic Non-Healing Wounds, Int. J. Burns. Trauma 2 (3) (2012) 126.
[13] M. Contardi, D. Russo, G. Suarato, J.A. Heredia-Guerrero, L. Ceseracciu, I. Penna, N. Margaroli, M. Summa, R. Spanò, G. Tassistro, L. Vezzulli, T. Bandiera, R. Bertorelli, A. Athanassiou, I.S. Bayer, Polyvinylpyrrolidone/Hyaluronic Acid-Based Bilayer Constructs for Sequential Delivery of Cutaneous Antiseptic and Antibiotic, Chem. Eng. J. 358 (2019) 912–923, https://doi.org/10.1016/J.CEJ.2018.10.048.
[14] R.S. Howell-Jones, M.J. Wilson, K.E. Hill, A.J. Howard, P.E. Price, D.W. Thomas, A Review of the Microbiology, Antibiotic Usage and Resistance in Chronic Skin Wounds, J. Antimicrob. Chemother. 55 (2) (2005) 143–149, https://doi.org/10.1093/JAC/DKH513.
[15] C. Li, R. Ye, J. Bouckaert, A. Zurutuza, D. Drider, T. Dumych, S. Paryzhak, V. Vovk, R.O. Bilyy, S. Melinte, M. Li, R. Boukherroub, S. Szunerits, Flexible Nanoholey Patches for Antibiotic-Free Treatments of Skin Infections, ACS Appl. Mater. Interfaces 9 (42) (2017) 36665–36674, https://doi.org/10.1021/ACSAMI.7B12949/ASSET/IMAGES/LARGE/AM-2017-12949E_0009.JPEG.

[16] B.S. Atiyeh, S.A. Dibo, S.N. Hayek, Wound Cleansing, Topical Antiseptics and Wound Healing, Int. Wound J. 6 (6) (2009) 420, https://doi.org/10.1111/J.1742-481X.2009.00639.X.
[17] A. Punjataewakupt, S. Napavichayanun, P. Aramwit, The Downside of Antimicrobial Agents for Wound Healing, Eur. J. Clin. Microbiol. Infect. Dis. 38 (1) (2019) 39–54, https://doi.org/10.1007/S10096-018-3393-5.
[18] Y. Zheng, N. Pan, Y. Liu, X. Ren, Novel Porous Chitosan/N-Halamine Structure with Efficient Antibacterial and Hemostatic Properties, Carbohydr. Polym. 253 (2021), 117205, https://doi.org/10.1016/J.CARBPOL.2020.117205.
[19] F. Hui, C. Debiemme-Chouvy, Antimicrobial N-Halamine Polymers and Coatings: A Review of Their Synthesis, Characterization, and Applications, Biomacromolecules 14 (3) (2013) 585–601, https://doi.org/10.1021/bm301980q.
[20] F. Wang, L. Huang, P. Zhang, Y. Si, J. Yu, B. Ding, Antibacterial N-Halamine Fibrous Materials, *Compos. Commun.* 22 (2020), 100487, https://doi.org/10.1016/J.COCO.2020.100487.
[21] R. Kaur, S. Liu, Antibacterial Surface Design – Contact Kill, Prog. Surf. Sci. 91 (3) (2016) 136–153, https://doi.org/10.1016/J.PROGSURF.2016.09.001.
[22] Y. Gao, N. Song, W. Liu, A. Dong, Y.J. Wang, Y.W. Yang, Construction of Antibacterial N-Halamine Polymer Nanomaterials Capable of Bacterial Membrane Disruption for Efficient Anti-Infective Wound Therapy, Macromol. Biosci. 19 (4) (2019) 1800453, https://doi.org/10.1002/MABI.201970010.
[23] A. Dong, Y.J. Wang, Y. Gao, T. Gao, G. Gao, Chemical Insights into Antibacterial N-Halamines, Chem. Rev. 117 (6) (2017) 4806–4862, https://doi.org/10.1021/acs.chemrev.6b00687.
[24] W. Chen, Y. Zhu, Z. Zhang, Y. Gao, W. Liu, Q. Borjihan, H. Qu, Y. Zhang, Y. Zhang, Y.J. Wang, L. Zhang, A. Dong, Engineering a Multifunctional N-Halamine-Based Antibacterial Hydrogel Using a Super-Convenient Strategy for Infected Skin Defect Therapy, Chem. Eng. J. 379 (2020), 122238, https://doi.org/10.1016/J.CEJ.2019.122238.
[25] R. Mastrangelo, D. Chelazzi, G. Poggi, E. Fratini, L.P. Buemi, M.L. Petruzzellis, P. Baglioni, Twin-Chain Polymer Hydrogels Based on Poly(Vinyl Alcohol) as New Advanced Tool for the Cleaning of Modern and Contemporary Art, Proc. Natl. Acad. Sci. U S A (2020), https://doi.org/10.1073/pnas.1911811117.
[26] V. Rosciardi, D. Chelazzi, P. Baglioni, "Green" Biocomposite Poly (Vinyl Alcohol)/Starch Cryogels as New Advanced Tools for the Cleaning of Artifacts, J. Colloid. Interface Sci. 613 (2022) 697–708, https://doi.org/10.1016/j.jcis.2021.12.145.
[27] J. Taktikos, H. Stark, V. Zaburdaev, How the Motility Pattern of Bacteria Affects Their Dispersal and Chemotaxis, PLoS One 8 (12) (2013) e81936.
[28] V. Sourjik, N.S. Wingreen, Responding to chemical gradients: bacterial chemotaxis, Curr. Opin. Cell Biol. 24 (2) (2012) 262–268, https://doi.org/10.1016/j.ceb.2011.11.008.
[29] D. Legland, I. Arganda-Carreras, P. Andrey, MorphoLibJ: Integrated Library and Plugins for Mathematical Morphology with ImageJ, Bioinformatics 32 (22) (2016) 3532–3534, https://doi.org/10.1093/bioinformatics/btw413.
[30] G. Bassu, M. Laurati, E. Fratini, Microgel Dynamics within the 3D Porous Structure of Transparent PEG Hydrogels, Colloids Surf. B Biointerfaces 221 (2023), 112938, https://doi.org/10.1016/J.COLSURFB.2022.112938.
[31] S.C. Edington, J.C. Flanagan, C.R. Baiz, An Empirical IR Frequency Map for Ester C=O Stretching Vibrations, J. Phys. Chem. A 120 (22) (2016) 3888–3896, https://doi.org/10.1021/acs.jpca.6b02887.
[32] F. Hui, C. Debiemme-Chouvy, Antimicrobial N-Halamine Polymers and Coatings: A Review of Their Synthesis, Characterization, and Applications, Biomacromolecules 14 (3) (2013) 585–601, https://doi.org/10.1021/bm301980q.
[33] Y. Liang, X. Zhao, P.X. Ma, B. Guo, Y. Du, X. Han, PH-Responsive Injectable Hydrogels with Mucosal Adhesiveness Based on Chitosan-Grafted-Dihydrocaffeic Acid and Oxidized Pullulan for Localized Drug Delivery, J. Colloid Interface Sci. 536 (2019) 224–234, https://doi.org/10.1016/J.JCIS.2018.10.056.
[34] L. Boulos, M. Prévost, B. Barbeau, J. Coallier, R. Desjardins, LIVE/DEAD(®) BacLight(TM): Application of a New Rapid Staining Method for Direct Enumeration of Viable and Total Bacteria in Drinking Water, J. Microbiol. Methods 37 (1) (1999) 77–86, https://doi.org/10.1016/S0167-7012(99)00048-2.
[35] Y. Deng, L. Wang, Y. Chen, Y. Long, Optimization of Staining with SYTO 9/Propidium Iodide: Interplay, Kinetics and Impact on Brevibacillus Brevis, Biotechniques 69 (2) (2020) 89–99, https://doi.org/10.2144/BTN-2020-0036.
[36] F. Ou, C. Mcgoverin, S. Swift, F. Vanholsbeeck, Rapid and Cost-Effective Evaluation of Bacterial Viability Using Fluorescence Spectroscopy, Anal. Bioanal. Chem. 411 (2019) 3653–3663, https://doi.org/10.1007/s00216-019-01848-5.
[37] J. Schindelin, I. Arganda-Carreras, E. Frise, V. Kaynig, M. Longair, T. Pietzsch, S. Preibisch, C. Rueden, S. Saalfeld, B. Schmid, J.Y. Tinevez, D.J. White, V. Hartenstein, K. Eliceiri, P. Tomancak, A. Cardona, Fiji: An Open-Source Platform for Biological-Image Analysis, Nat. Methods 9 (7) (2012) 676–682, https://doi.org/10.1038/nmeth.2019.
[38] R.K. Tubbs, Sequence Distribution of Partially Hydrolyzed Poly(Vinyl Acetate), J. Polym. Sci. A1 4 (3) (1966) 623–629, https://doi.org/10.1002/POL.1966.150040316.
[39] G. van der Velden, J. Beulen, 300-MHz 1H NMR and 25-MHz 13C NMR Investigations of Sequence Distributions in Vinyl Alcohol-Vinyl Acetate Copolymers, Macromolecules 15 (4) (1982) 1071–1075, https://doi.org/10.1021/MA00232A022.
[40] B.D. Coleman, T.G. Fox, General Theory of Stationary Random Sequences with Applications to the Tacticity of Polymers, J Polym Sci A 1 (10) (1963) 3183–3197, https://doi.org/10.1002/POL.1963.100011013.
[41] A. Lederer, J. Brandt, Multidetector Size Exclusion Chromatography of Polymers in Malik, in: M.I., J. Mays, M.R. Shah (Eds.), *Molecular Characterization of Polymers: A Fundamental Guide* **2021**, 61–96. https://doi.org/10.1016/B978-0-12-819768-4.00012-9.
[42] J.C.J.F. Tacx, H.M. Schoffeleers, A.G.M. Brands, L. Teuwen, Dissolution Behavior and Solution Properties of Polyvinylalcohol as Determined by Viscometry and Light Scattering in DMSO, Ethyleneglycol and Water. *Polymer* 41 (3) (2000) 947–957, https://doi.org/10.1016/S0032-3861(99)00220-7.
[43] G.O. Ildiz, I. Boz, O. Unsalan, FTIR Spectroscopic and Quantum Chemical Studies on Hydantoin, Optics and Spectroscopy (english Translation of Optika i Spektroskopiya) 112 (5) (2012) 665–670, https://doi.org/10.1134/S0030400X12050062.
[44] D.R. Picout, S.B. Ross-Murphy, Rheology of Biopolymer Solutions and Gels, Sci. World J. 3 (2003) 105–121, https://doi.org/10.1100/TSW.2003.15.
[45] V. Rosciardi, P. Baglioni, Role of Amylose and Amylopectin in PVA-Starch Hybrid Cryo-Gels Networks Formation from Liquid-Liquid Phase Separation, J. Colloid. Interface Sci. 630 (2023) 415–425, https://doi.org/10.1016/J.JCIS.2022.10.092.
[46] V.Y. Rudyak, D.E. Larin, E.N. Govorun, Microphase Separation of Statistical Multiblock Copolymers, Macromolecules 55 (21) (2022) 9345–9357, https://doi.org/10.1021/ACS.MACROMOL.2C00065.
[47] V.I. Lozinsky, Cryostructuring of Polymeric Systems. Cryogels and Cryotropic Gel-Formation: Terms and Definitions, *Gels* 4 (3) (2018) 77, https://doi.org/10.3390/gels4030077.
[48] X. Yan, Z. Jie, L. Zhao, H. Yang, S. Yang, J. Liang, High-Efficacy Antibacterial Polymeric Micro/Nano Particles with N-Halamine Functional Groups, Chem. Eng. J. 254 (2014) 30–38, https://doi.org/10.1016/J.CEJ.2014.05.114.
[49] B. Ye, Y. Li, Z. Chen, Q.Y. Wu, W.L. Wang, T. Wang, H.Y. Hu, Degradation of Polyvinyl Alcohol (PVA) by UV/Chlorine Oxidation: Radical Roles, Influencing Factors, and Degradation Pathway, Water. Res. 124 (2017) 381–387, https://doi.org/10.1016/J.WATRES.2017.05.059.
[50] H.S. Mansur, C.M. Sadahira, A.N. Souza, A.A.P. Mansur, FTIR Spectroscopy Characterization of Poly (Vinyl Alcohol) Hydrogel with Different Hydrolysis Degree and Chemically Crosslinked with Glutaraldehyde, Mater. Sci. Eng. C 28 (4) (2008) 539–548, https://doi.org/10.1016/J.MSEC.2007.10.088.
[51] M. Natan, O. Gutman, R. Lavi, S. Margel, E. Banin, Killing Mechanism of Stable N-Halamine Cross-Linked Polymethacrylamide Nanoparticles That Selectively Target Bacteria, ACS Nano 9 (2) (2015) 1175–1188, https://doi.org/10.1021/NN507168X.
[52] Q. Chen, Q. Ding, W. Li, J. Deng, Q. Lin, J. Li, Enhanced Treatment of Organic Matters in Starch Wastewater through *Bacillus subtilis* Strain with Polyethylene Glycol-Modified Polyvinyl Alcohol/Sodium Alginate Hydrogel Microspheres, Bioresour. Technol. 347 (2022), 126741, https://doi.org/10.1016/J.BIORTECH.2022.126741.
[53] T. Hölscher, B. Bartels, Y.C. Lin, R. Gallegos-Monterrosa, A. Price-Whelan, R. Kolter, L.E.P. Dietrich, Á.T. Kovács, Motility, Chemotaxis and Aerotaxis Contribute to Competitiveness during Bacterial Pellicle Biofilm Development, J. Mol. Biol. 427 (23) (2015) 3695–3708, https://doi.org/10.1016/J.JMB.2015.06.014.